Surface & Coatings Technology 483 (2024) 130711

Contents lists available at ScienceDirect

Surface & Coatings Technology

journal homepage: www.elsevier.com/locate/surfcoat

A predictive modeling approach for cold spray metallization on polymers

Jung-Ting Tsai [a,*], Semih Akin [b], David F. Bahr [c], Martin Byung-Guk Jun [d]

[a] Department of Mechanical Engineering, National Taiwan University of Science and Technology, Taipei 106335, Taiwan
[b] Department of Mechanical, Aerospace and Nuclear Engineering, Rensselaer Polytechnic Institute, Troy, NY 12180, USA
[c] School of Materials Engineering, Purdue University, West Lafayette, IN 47907, USA
[d] School of Mechanical Engineering, Purdue University, West Lafayette, IN 47907, USA

ARTICLE INFO

Keywords:
Cold spray
Polymer metallization
Three-network polymer model
Numerical modeling
Predictive modeling
Finite element analysis

ABSTRACT

Cold spray (CS) particle deposition, also known as cold spray additive manufacturing, presents opportunities for high-throughput functional metallization on polymeric substrates. However, modeling CS-based polymer metallization and quantifying deposition probability face challenges due to the need for dedicated and cost-intensive experimental characterization tools. This underscores a critical need for predictive approaches such as numerical modeling. Toward this end, the present work aims to address this critical gap through numerical modeling by utilizing the three-network polymer model (TNM) in a manner that deposition probability can be predicted under the given CS process settings. In this regard, CS of both hard and soft particles with varying densities and diameters was modeled, followed by experimental validation. Notably, a dimensional number (η) – representing the fraction of the particle kinetic energy - was derived as a predictive tool to estimate the CS metallization probability on polymeric substrates. Furthermore, the modeling endeavor was extended to develop a correlation between the η number and the percent area coverage of the CS process. It was found that η value should be higher than 0.8 for effective CS polymer metallization. Controlled experiments confirmed the viability and reliability of the numerical modeling as a high-fidelity predictive methodology for the CS metallization on polymers, thereby minimizing the need for cost-intensive trial-and-error efforts.

1. Introduction

Cold spray (CS) has been initially developed for material repair and restoration [1]. However, with recent innovations, the application domain of CS has exponentially grown in multiple areas, including solid-state additive manufacturing, polymer metallization, energy devices, and even in biomaterial and sensor applications [2]. Furthermore, surface deposition using heterogeneous (hybrid) materials can be accomplished via CS under controlled process parameters [3–6]. This pivotal feature of the CS has paved the way for metallization on polymeric substrates, offering functional surface structures for a diverse array of applications domains, including printed electronics, antibacterial surfaces, energy devices, etc. [7–9].

Despite the significant advances, several critical challenges remain to effectively CS functional metal particles onto polymer targets. These challenges involve: (i) severe plastic deformation of the soft polymer substrate under the high-speed impingement of metal particles [5,10,11]; and (ii) erosion of the as-cold sprayed (as-CS) layer under the impact of subsequent particles [12,13]. These factors collectively hinder the thick-layer CS particle deposition on polymeric substrates. The initial coated layer is crucial as it establishes mechanical interlocking between the as-CS particles and polymer substrate. This stage of CS is responsible for achieving effective functional metallization on polymeric substrates. During this stage, the impact velocity of particles is generally lower than that for subsequent layers. This is because the first layer does not require the particle to undergo plastic deformation but rather to be embedded (i.e., mechanically interlocked) into the substrate. As such, a fundamental understanding of the first-layer build-up mechanism of CS on polymers is imperative to unlock the remarkable potential of this emerging manufacturing technique across diverse application domains.

Previous efforts mainly focused on experimentally understanding the first-layer CS build-up on polymers, considering a specific set of CS operational settings tailored for specified target materials [14,15]. Despite significant advances, challenges and shortcomings persist, stemming from the need for dedicated adjustments and calibration of the materials, process settings, and experimental setups. For example, variations in the mechanical properties of polymer substrates alter the critical impact velocity of particles required for successful metallization

* Corresponding author at: No.43, Keelung Rd., Sec.4, Da'an Dist., Taipei City 106335, Taiwan.
E-mail address: tsaij@mail.ntust.edu.tw (J.-T. Tsai).

https://doi.org/10.1016/j.surfcoat.2024.130711
Received 13 December 2023; Received in revised form 15 March 2024; Accepted 23 March 2024
Available online 2 April 2024

Nomenclature

Symbol

d_p	diameter of particle
F_A^e	elastic deformation gradient of network A
J_A^e	determinant of the elastic deformation gradient of network A
$\lambda_A^{e^*}$	elastic chain stretch
$b_A^{e^*}$	Cauchy-Green deformation tensor of network A
L^{-1}	Inverse Langevin function
μ_A	shear modulus of network A
μ_C	shear modulus of network C
λ_L	chain locking stretch
μ_{Bi}	initial shear modulus of network B
μ_{Bf}	final shear modulus of network B
V_r	particle rebound velocity
r_p	radius of particle
η	kinetic energy fraction
V_{in}	initial particle velocity

Abbreviation

CS	cold spray
Cu	copper
FEA	finite element analysis
JK	Johnson-Cook
MZA	Modified Zerilli Armstrong
PTK	Preston Tonk Wallace
SEM	scanning electronic microscopy
Sn	tin
TNM	three-network model
TNVM	three-network viscoplastic model

[12,16,17]. Specifically, particles undergo high-speed impact onto the substrate, leading to high strain rate of plastic deformation of the polymer substrate. Experimentally capturing high strain-rate (10^6 s^{-1}) deformation in CS poses challenges. Hence, this impedes comprehensive investigations on the first-layer CS build-up on polymers, especially when considering a wide range of functional particles and substrate materials. This underscores the need for alternative predictive, cost-effective and affordable methodologies based on numerical modeling approaches.

In the literature, the numerical modeling efforts of CS mainly lie in six constitutive models that describe high-strain rate plasticity under metal-to-metal impact [18–21]. The models include the Johnson-Cook (JC) plasticity model, Modified Zerilli Armstrong (MZA), Voyiadjis Abed (VA), Preston Tonk Wallace (PTW), Modified Khan Huang Liang (MKHL), and Gao Zhang (GZ) models. However, these models are suitable for metal substrates using metal particles, as they simulate material consolidation. Due to the high-strain plastic deformation of soft substrates, such as polymers, these models cannot effectively capture the mechanical interlocking of the metal particles with the polymer substrate [18,22–26].

On the other hand, the response of polymer in high strain rate deformation is studied extensively, including testing equipment such as

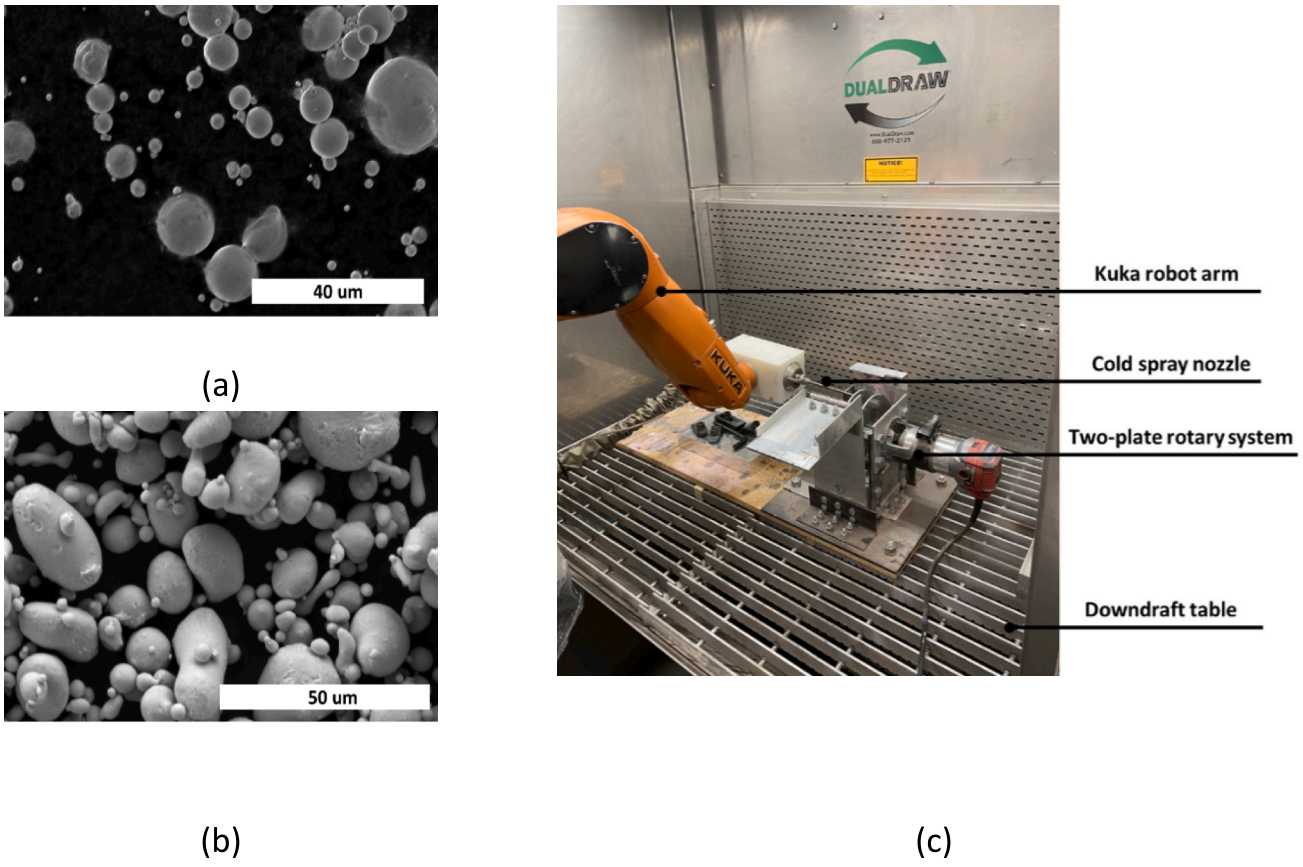

Fig. 1. Morphology of (a) Cu powders; (b) Sn powders; (c) cold spray setup (left) with the two-plate rotary system (right).

Table 1
Feedstock powders used in this study.

Powders	Vendor	Powder size distribution (μm)			Density (g/cm^3)
		D (0.1)	D (0.5)	D (0.9)	
Tin (Sn)	CenterLine	1.5	6.5	15	7.31
Copper (Cu)	Chemical Store Inc	22	32	41	8.96

Hopkinson bar, Taylor impact, and transverse impact, which is implemented in various strain rate testing to observe the response of polymers [25,27–30]. A time-temperature superposition for predicting the high strain rate polymer response was accomplished with a low strain rate input. Church et al. [31] proposed a thermomechanical model that considers the effect of temperature, strain rate, and pressure to examine the flow rule, the strain-softening mechanism, and the orientation hardening. The simulation results showed good agreement with the experimental results from the polymeric substrates such as PMMA and PC. Sarva et al. [28] conducted a study considering two types of polymers, PC and PVDF, and showed increased strain-rate with the increased temperature. The yield stress showed a bilinear behavior depending on the strain rate scale. The phenomenon was caused by the PC beta transition and the PVDF glass transition at a strain rate of 0.001 to 5000 s^{-1}. Although extensive studies have been conducted, the implications of applying CS metallization on polymers have not been extensively explored. Moreover, a critical need remains for numerical modelings that capture polymer metallization with high fidelity, predicting the deposition efficiency and probability without the need for dedicated experimental tools.

To this end, this study addresses this crucial gap by proposing a numerical modeling framework to model the CS impact of metal particles on a polymer substrate. The primary goal is to develop a predictive modeling framework that enables capturing deposition efficiency and probability of the CS process, ultimately contributing to the optimization of CS polymer metallization with minimal trial and error efforts. In this regard, a calibrated three-network polymer model is employed to simulate the high strain-rate deformation of the polymer substrate, followed by experimental validation. Subsequently, a dimensional number (η) – representing the fraction of the particle kinetic energy - is derived as a predictive tool to estimate the CS deposition probability on polymeric substrates, accounting for varying particle density and sizes. Lastly, the numerical modeling is extended to establish a correlation between the η number and the percent area coverage of the CS metallization process under the specified CS process settings. The main contribution of this work lies in developing a numerical framework that allows high-fidelity prediction of the CS metallization for a broad spectrum of metallic micro-particles in an affordable manner by minimizing the trial-and-error efforts.

2. Materials and methods

Two different feedstock materials, namely copper (Cu) and Tin (Sn),

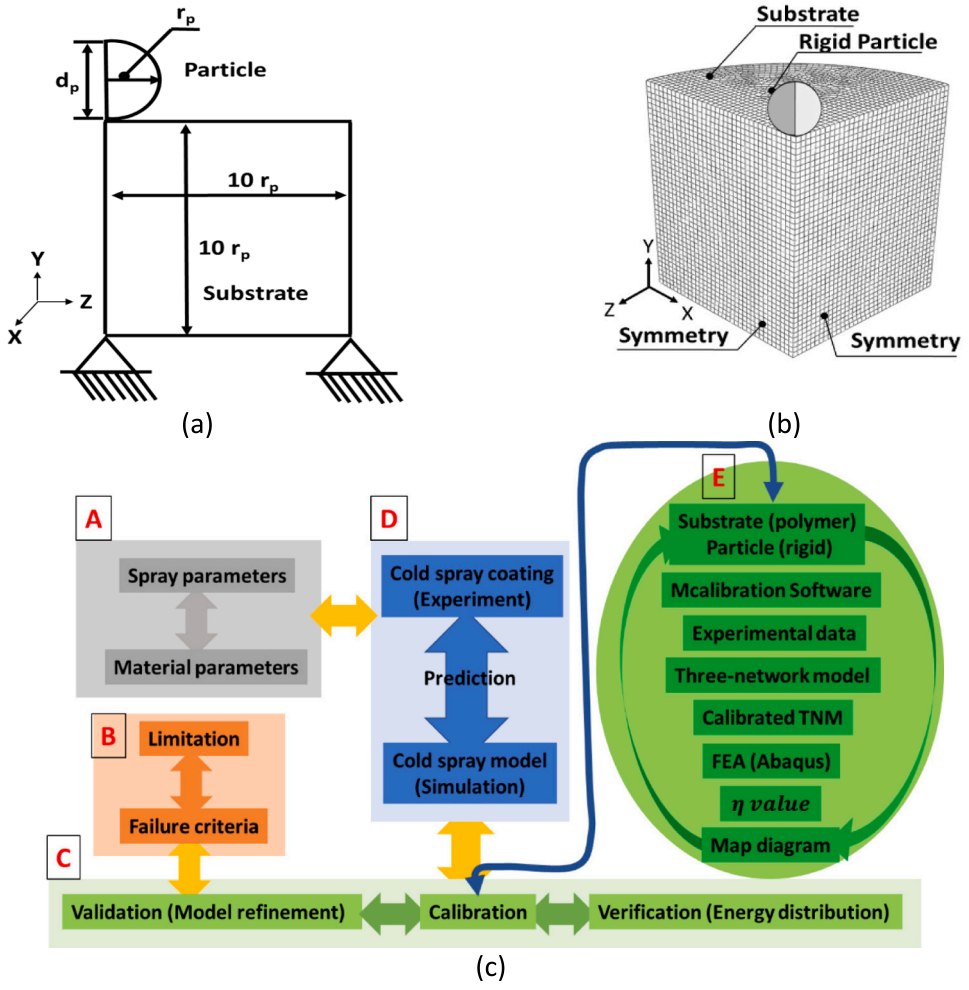

Fig. 2. (a) Boundary conditions for the simulated model (b) The designed geometry with meshed structure; (c) research workflow of the study.

Table 2
A list of constitutive viscoplastic models.

	Comments	Ref.
Model for metals		
Johnson-Cook (JK)	Commonly used for metal plasticity deformation but limited for high strain rate response.	[19]
Modified Zerilli Armstrong (MZA)	Incorporate various parameters for simulating high strain rate material but limited for specific materials at certain conditions.	[37]
Voyiadjis Abed (VA)	Aim to capture nonlinear and rate-dependent material behavior in high-speed deformation, considering strain-rate sensitivity, temperature effects, and strain hardening.	[38]
Preston Tonk Wallace (PTW)	Considers strain sensitivity, thermal softening and strain hardening.	[39]
Gao Zhang (GZ)	Good at predicting high strain rates $>10^4\ s^{-1}$	[40]
Model for polymers		
Neo-Hookean	A simple hyperelastic model that simulates large deformations but unsuitable for large-range strain changes.	[41]
Arruda-Boyce	Developed for large strain, time and temperature response for glassy polymers.	[42,43]
Hybrid	Developed for predicting large stain time-dependent of ultra-high molecular polyethylene, also able to respond to other types of thermoplastics.	[44]
Three Network	It's an extension development of the Hybrid model for thermoplastic materials	[36]
Three Network Viscoplastic	The model is a general form that uses 1, 2, or 3 parallel networks to capture the experimental behavior of thermoplastic deformation.	[45]

were employed in the CS experiments. As shown in SEM images (FEI, Quanta 650 FESEM) in Fig. 1a-b, powders exhibit quasi-spherical morphology, with a size distribution ranging from 10 to 50 μm. Table 1 presents the feedstock particle information. Cu and Sn particles were chosen to investigate the impingement of hard (Cu) and relatively soft (Sn) powders into the polymer target, with the aim that the numerical modeling can be calibrated for powders with various densities.

A low-pressure CS system (Rus Sonic Technonolgoy, Model: K205/407R), as shown in Fig. 1(c), was used in the experiment. Various inlet pressures (0.5 MPa- 0.7 MPa) were applied to the CS system at room temperature (25 $^{\circ}C$) using compressed air as the driving gas. The CS gun was mounted on a programmable robot arm (Kuka Agilus) for high-precision coating experiments.

The nozzle stand-off distance was set to 30 mm and the nozzle transverse speed was 0.1 mm/s. Three sets of particle impact velocities (i.e., 200 m/s, 300 m/s, 400 m/s) were considered onto the Nylon substrate (polyamide 6,6, ePlastic Co., USA), with a thickness of 813 μm. The impact velocity of particles was measured using a two-plate rotary system setup (see Fig. 1(a)). Detailed information regarding the two-plate rotary system setup and the particle impact velocity calculation methodology can be found in [32,33]. The Nylon substrates were prepared according to the ASTM D638-14 standard [34].

3. Numerical modeling

The CS particle deposition was modeled using a commercial computational package (Abaqus 2018). The single particle impact was simulated through the Lagrangian approach, considering the metal particles (i.e., Cu, Sn) are impinging into the target polymer substrate. Fig. 2(a) shows the finite element (FE) modeling domain and relevant boundary conditions. In detail, the axisymmetric boundary condition was applied to the modeling due to the nature of the axisymmetric geometry, enabling a reduction in computational time. Symmetry boundary conditions were applied to both the X-plane and the *Z*-plane. Consequently, the bottom substrate is encastre, while the surfaces on both sides are symmetric.

Fig. 2(b) shows the computational domain meshed with hexahedral elements. The particle in this research is assumed to be rigid. The particle-to-substrate length ratio was kept at 1:5 to ensure a grid-independent solution. As for the inlet boundary conditions, the particle impact velocity was assigned to the model. The particles' impact velocity was experimentally determined through the two-plate rotary system setup [32,33] and then integrated into the numerical modeling. The particle impingement was treated as an adiabatic process, and the model was defined through C3D8R for all cases (i.e., representing the average strain of an 8-node linear brick with reduced integration). A node-to-surface method was employed to simulate the interactions between the impinging particle and the substrate. A hard contact model was also utilized to account for the pressure-overclosure relationship between the particle and the polymer interface, enabling the particle to impinge into the substrate upon impact. The Coulomb friction model was used to model the friction between the particle and the substrate, which is fixed at 0.25. The detailed simulation model setup can be found in Tsai [35].

Several plasticity models exist in the literature to simulate the high-strain deformation of the polymer substrate. Table 2 lists these models, presenting their pros and cons in the domain of high-strain viscoplastic deformation. Among others, the three-network polymer model (TNM) can effectively capture the polymer substrate's high-strain deformation under the particles' high-speed impingement [36]. In this regard, TNM was employed to simulate the CS particle deposition on the polymer target effectively. The governing equations of each network are given in Eqs. (1)–(3).

$$\sigma_A = \frac{\mu_A}{J_A^e \underline{\lambda}_A^{e^*}} * \frac{L^{-1}\left(\frac{\underline{\lambda}_A^{e^*}}{\lambda_L}\right)}{L^{-1}\left(\frac{1}{\lambda_L}\right)} * dev\left[b_A^{e^*}\right] + \kappa\left(J_A^e - 1\right)I \tag{1}$$

$$\sigma_B = \frac{\mu_B}{J_B^e \underline{\lambda}_B^{e^*}} * \frac{L^{-1}\left(\frac{\underline{\lambda}_B^{e^*}}{\lambda_L}\right)}{L^{-1}\left(\frac{1}{\lambda_L}\right)} * dev\left[b_B^{e^*}\right] + \kappa\left(J_B^e - 1\right)I \tag{2}$$

$$\sigma_C = \frac{\mu_C}{J\,\lambda_{chain}} * \frac{L^{-1}\left(\frac{\lambda_{chain}}{\lambda_L}\right)}{L^{-1}\left(\frac{1}{\lambda_L}\right)} * dev\left[b^{e^*}\right] + \kappa(J-1)I \tag{3}$$

where $J_A^e = det\left[F_A^e\right]$, $b_A^{e^*} = J_A^{e\,-2/3} F_A^e \left(F_A^e\right)^T$, $\underline{\lambda}_A^{e^*} = \left(tr\left[b_A^{e^*}/3\right]^{1/2}\right)$, $L(x) = coth(x) - \frac{1}{x}$μ, μ_A and μ_C is the shear modulus of network A and network C, λ_L is the locking stretch, μ_{Bi} and μ_{Bf} are the initial and final shear modulus of network B, and κ is the bulk modulus.

To elaborate, the initial deformation of the semi-crystalline and the amorphous domain is described by the first two parallel networks, A and B. The third network, C, delineates the polymer target's significant strain under the particle's impingement, ultimately enabling the accurate representation of high-strain plastic deformation in the target polymer substrate. Notably, the TNM necessitates rigorous calibration of material constants to capture the high-strain deformation [27–34] effectively. In this work, TNM was particularly calibrated for the polyamide substrate using high-speed dynamic test tools-Split-Hapkinson Bar technique [31]. Detailed information regarding the model calibration setup and the methodology can be found in [33].

Fig. 2c presents the workflow for predicting the CS metallization on the polymer target. The work can be separated into five blocks alphabetically from A to E. Block A shows the controlling process, spray, and material parameters. Calibration involves adjusting the material constants in the model to capture the polymer deformation phenomenon. Verification ensures the model's stability and energy balance, while

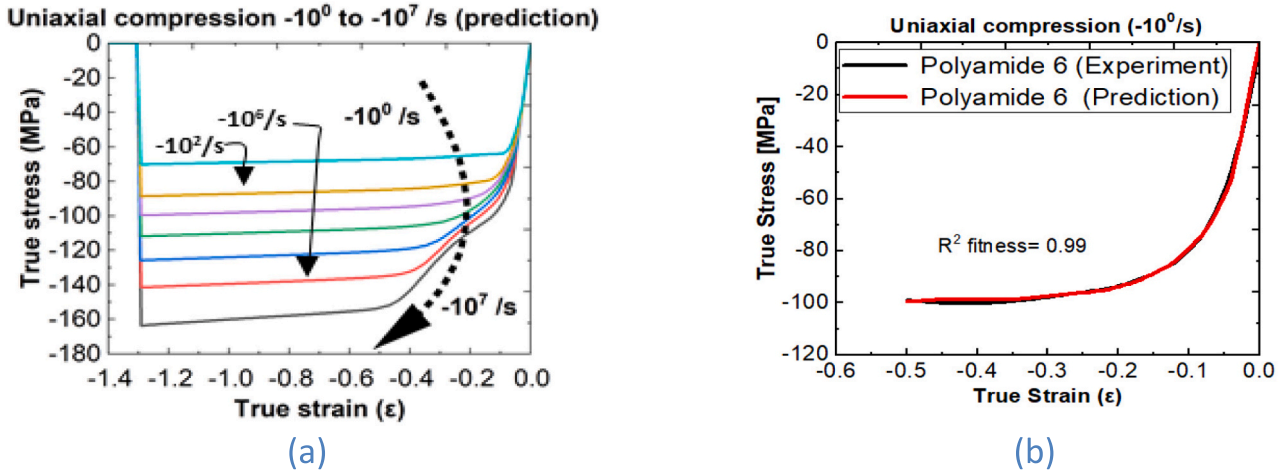

Fig. 3. (a) The output strain rate from -10^0 to -10^7/s (b) The simulated and experimental true stress response of the Nylon substrate under uniaxial compression strain (-10^3 s^{-1}).

validation involves refinements such as mesh, fracture criteria, etc. Achieving model accuracy requires increased computational time and resources, thus necessitating a balance between accuracy and input expenditure, which is addressed in Block B. Block C illustrates the simulation model undergoing three steps: calibration, verification, and validation. Block D represents the comparison of the CS model output prediction with experimental results. Block E outlines the detailed process of the calibration model. This research assumes the particle is rigid while the substrate uses the (Three-network model) TNM. A commercial-ready software-Mcalibration, is used to determine the material constants by inputting experimental data. After calibration, the substrate is generated in Abaqus software for CS simulation studies. Each case is conducted separately to collect the η values, which are then plotted together as a map diagram.

Fig. 3(a) shows true strain versus true stress under a wide range of uniaxial compression strain rates ranging from -10^0 to -10^7/ s. The results consistently demonstrate an increase in true stress as the strain rate rises, confirming the stability of the simulations. Fig. 3(b) shows the calibrated TNM for the Nylon substrate at a fixed uniaxial compression strain rate (-10^3 s^{-1}). The simulated results align with the trends observed in high-strain rate compression experiments, displaying a reliable fit (i.e., the coefficient of determination (R^2) = 0.99). Furthermore, the results reveal that the calibrated TNM effectively captured the Nylon's compression state rate response. These findings suggest that the calibrated TNM model is reliable for conducting particle impingement simulations for the CS process.

To solve numerical modeling for CS metallization, certain assumptions have been made and are summarized as follows:

i. Particles are assumed to be spherical, rigid, and within 10–50 μm.
ii. Particles' impact the target substrte at room temperature (25 $^{\circ}C$).
iii. Particles and target substrate are modeled axisymmetrically.
iv. Particle impact process is adiabatic, and total energy is preserved during the impact.

Acknowledging these assumptions, the numerical model was collectively solved to simulate the particle-substrate interactions. The ultimate goal is to develop a metric that predicts the deposition probability for CS metallization on polymers.

4. Results and discussion

Fig. 4(a) presents the energy distribution of a Cu particle impacting the polymer substrate. The impingement process is adiabatic, wherein the total energy is conserved. Noteworthy is that the total energy comprises the sum of the particle's kinetic energy and internal energy. The internal energy encompasses plastic dissipation energy, strain energy, artificial energy, and friction energy (i.e., total energy = kinetic energy + internal energy (plastic dissipation energy + strain energy + artificial energy (i.e., the control of hourglass deformation) + friction energy). The total energy is constant with increasing time, demonstrating that the energy is conserved (the simulation converges). The plastic dissipation energy increases significantly with the decrease of kinetic energy due to the severe plastic deformation of the substrate. Over time, the strain energy recovers, accompanied by an increase in the kinetic energy—this energy recovery results in particles rebounding from the polymer surface.

By utilizing the kinetic energy transfer of the particles before and upon impact, a dimensionless number (η) can be derived to correlate the kinetic energy fraction as given in Eq. (4), where V_{in} is the particle velocity and V_r is the particle rebound velocity. As such, the η value can be potentially used to predict the CS deposition probability for polymer metallization. The η value provides a kinetic energy ratio ranging from 0 to 1. A higher η value indicates a greater likelihood of particles being embedded in the polymer substrate and vice versa.

$$\eta = \frac{V_{in}^2 - V_r^2}{V_{in}^2} \tag{4}$$

After calibrating the model, simulations were conducted, considering metal particles (i.e., Cu with 30 μm diameter) impinging on the polymer target at an impact velocity of 400 m/s. Fig. 4(b) presents the true strain versus true strain of the polymer target under the impingement of the Cu particles. Three strain failure thresholds (i.e., 0.6, 1, 1.4) were considered to simulate the high-strain polymer deformation. The elements are deleted when the failure criteria are satisfied to simulate the high-strain plastic deformation. Notably, the particle-polymer contact region deforms and fractures as the particle travels at an elevated velocity, exceeding the strain failure criteria. The failure parameters are done in this research to showcase the influence of the particle embedding into the polymer substrate. If the strain failure is satisfied, the particle is embedded inside the polymer target, resulting in an effective mechanical interlocking. Results show that as the Von Mises (true) strain increases, the particle for three cases is embedded in the polymer substrate. However, it is noticeable that the particle rebounds from the substrate after the particle impacts the polymer substrate. As the Von Mises (true) strain increases, the particle rebound in the polymer substrate increases.

Table 3 compares the impingement of the particle (Cu) into the

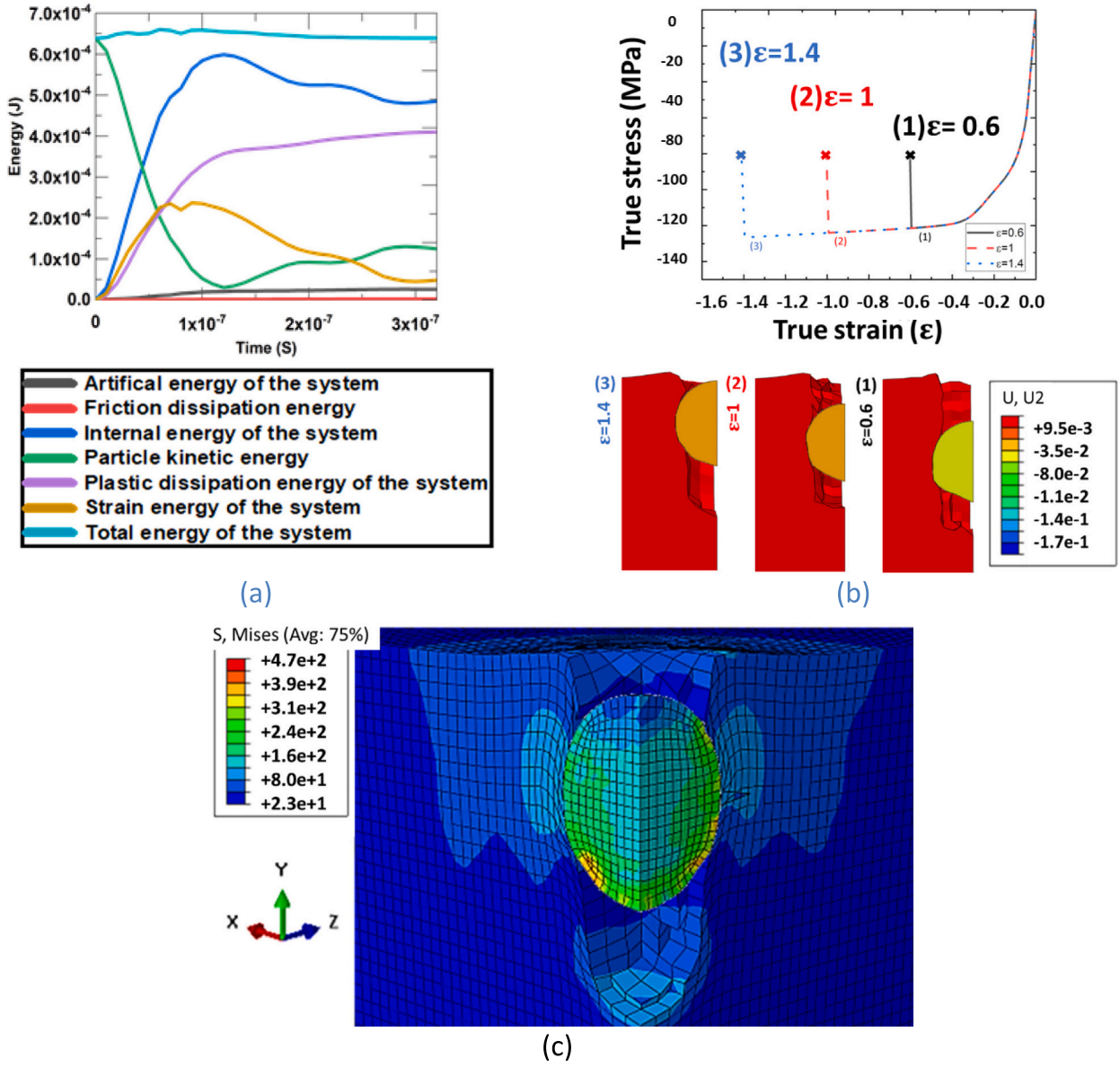

Fig. 4. (a) Total energy distribution under cold spraying of Cu particle on the Nylon target (The energy curve from up to down are: total energy, particle kinetic energy, internal energy, plastic dissipation energy, strain energy, artificial energy, and friction dissipation energy). (b) Failure criteria at strain 0.6, 1, and 1.4. (c) Particle interlocking by the polymer substrate.

Table 3
Materials damage criteria used in the numerical modeling.

Cases	Case 1	Case 2	Case 3
Von mises (true) strain (ε)	0.6	1	1.4
Relative CPU time	1	0.8	0.8
η value	1	1	1
Energy AE/IE	5.57	4.72	3.1

polymer (polyamide) substrate under the three different strain failure criteria, specifically at Von Mises (true) strains of 0.6, 1, and 1.4, respectively. The comparison was conducted by evaluating the relative CPU time (relative CPU time is defined as the time for case 1 to accomplish, dividing case 2 and case 3), the η value, and the energy AE/IE (artificial energy/internal energy). As the Von Mises (true) strain increases from 0.6 to 1.4, the energy ratio AE/IE decreases from 5.57 to 3.1. In this study, polymer failure is assumed to occur when the strain reaches 1 (case 2). This choice is grounded in the observation that case 1 exhibits the highest AE/IE energy, whereas cases 2 and 3 display the lowest. However, for case 3, the failure criteria for polymer Von Mises (true) strain reaching 1.4 are rarely encountered in engineering applications, especially at high-speed impacts. Therefore, considering relative CPU time, the η value, and the energy AE/IE, the conditions of case 2 are selected to simulate the high-strain rate deformation of CS particles in this research within the realm of polymer metallization.

Fig. 4(c) shows the particle impingement into the polymer target (i.e., Cu with 30 μm diameter at an impact velocity of 400 m/s), in which the contact region between the particle and the substrate undergoes plastic deformation. Upon meeting the failure criteria (Von Mises (true) strain at 1), elements interacting with the impinging particle are removed from the model, simulating high-strain rate deformation of the substrate. Furthermore, when the failure criteria are met, the impinging particle remains embedded in the polymer substrate, indicating successful mechanical interlocking of the particle by the polymer substrate.

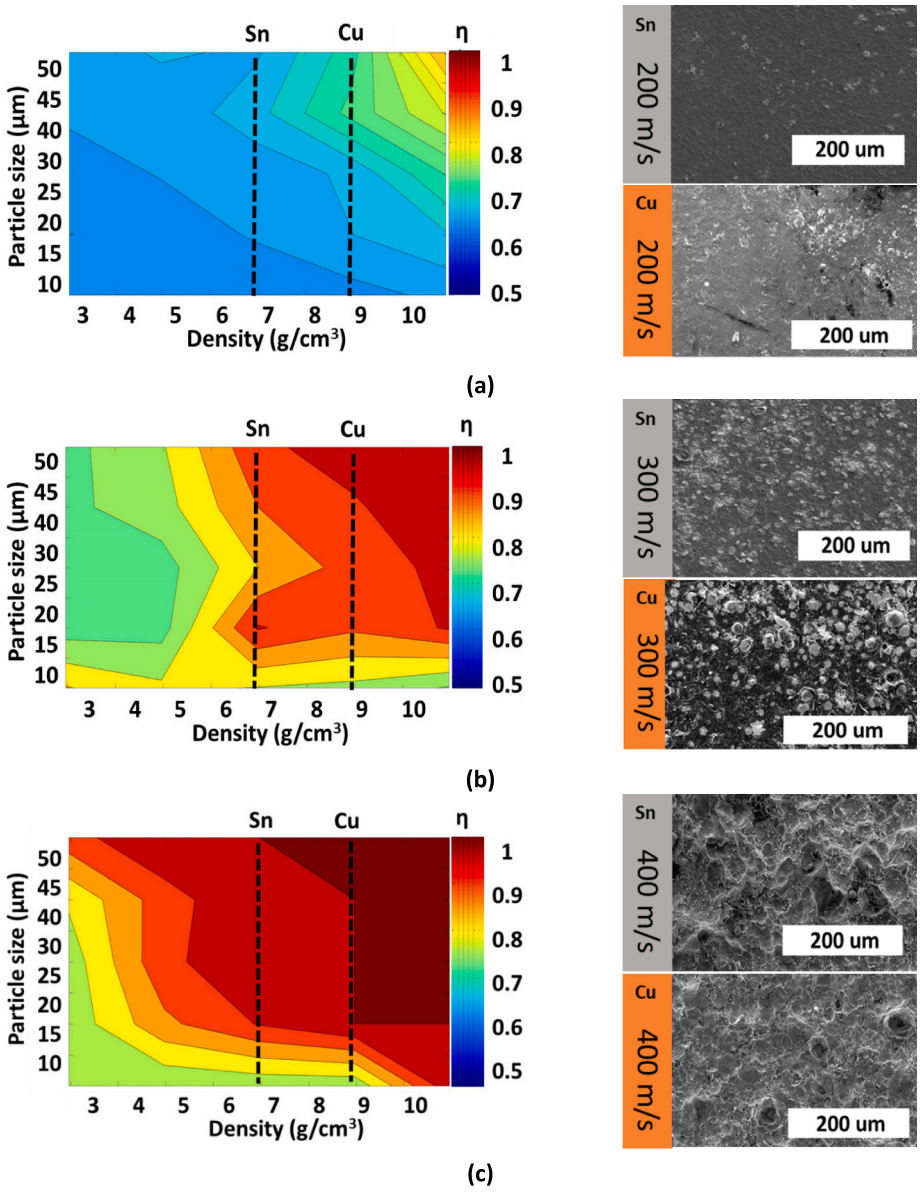

Fig. 5. Cold spray map diagrams considering different particle sizes and densities for metallization on Nylon (polyamide) substrate at various particle velocities: (a) 200 m/s; (b) 300 m/s; (c) 400 m/s.

Fig. 5(a-c) show the map diagrams of the CS impingement simulations at various particle impact velocities: 200 m/s, 300 m/s, and 400 m/s, respectively. In these diagrams, the x-axis represents particle density ranging from 2.95 to 10.95 g/cm^3, and the y-axis represents particle size, varying between 10 μm and 50 μm. The output of these plots is the rebound coefficient (η) for particles with different densities and sizes. As observed in each diagram, the η value increases with both particle velocity and size. It is attributed to the kinetic energy gain of the particles at higher impact velocity and larger sizes. This trend is more pronounced at higher particle impact velocities (400 m/s), leading to a higher η across a wide range of parameter spectra (see Fig. 5c). Microstructural characterizations in Fig. 5(a-c) also reveal that particles exhibit a greater tendency to adhere to the substrate at higher impact velocities, translating to elevated η values.

In detail, no significant particle deposition was observed when the particle impact velocity was 200 m/s, corresponding to $\eta < 0.8$. In this scenario, the particles tend to rebound from the surface without achieving deposition due to insufficient kinetic energy. Upon increasing the impact velocity to 300 m/s, a larger number of particles successfully impinged on the polymer surface, facilitated by the gained kinetic energy. Specifically, when $\eta > 0.8$, successful CS particle deposition on the polymer target is expected; conversely, if $\eta < 0.8$, the particles will tend to rebound from the surface, leading to unsuccessful metallization. At an impact velocity of 400 m/s, particles underwent metallurgical consolidation on the polymer surface, resulting in successful metallization. These observations are correct for both soft (Sn) and hard (Cu) particles (Sn is relatively softer than Cu; however, in this research, it is assumed that both particles are rigid and therefore, the simulation sets the density of Sn particles as 7.3 g/cm^3, while Cu is 8.96 g/m^3). Taken together, the η value can serve as a practical and effective metric for predicting deposition probability. The results agree well with the microstructural observations in Fig. 5(a-c). Hence, by utilizing the η value, a generalized deposition window can be defined for polymer metallization, accommodating a broad spectrum of functional metal particles with varying size distributions.

Furthermore, the modeling efforts can be extended to predict the overall deposition efficiency of the CS metallization by utilizing the η value. In detail, the area coverage of the resulting coating can be

Table 4
Summary of numerical modeling results and comparison with the CS experiments.

Particle	Sn			Cu		
Particle impact velocity (m/s)	200	300	400	200	300	400
η value	<0.8	0.8	>0.8	<0.8	0.85	>0.85
Particle size (μm)	11.38±4.64	10.78 ±4.39	Form coating layer	14.91±4.42	16.11 ±5.5	Form coating layer
Surface area coverage of particles (%)	<2	29.53	100	<1	25.35	100

Table 5
Published articles on polymer metallization via cold spray.

References	Feedstock powder	Average (D_{50}) powder size (μm)	Substrate material	Inlet gas pressure/particle impact velocity	Surface area coverage of particles (%)	η value[a]
Current work	Cu	32	PA6	0.7 MPa	100	>0.85
Current work	Sn	6.5	PA6	0.7 MPa	100	>0.8
[46]	Cu	5	PA6	0.5 MPa	22.05	<0.7
[47]	Sn	17	GFRP	0.7 MPa	100	>0.9
[10]	Sn	14	PA6	>400 m/s	100	>0.9

[a] η value was identified from Fig. 5 for the relevant experimental settings (only consider inlet pressure and assume the spray is at room temperature).

correlated with the η value to estimate the deposition probability along with the area coverage of deposited particles. In other words, the η value obtained from the single-particle impact can be extrapolated to estimate the probability of multi-particle CS surface deposition. In this regard, the area coverage of the particles in the SEM images in Fig. 5(a-c) was calculated using open-source image processing software (ImageJ). Table 3 shows the CS metallization metrics on the polymer (polyamide) substrate, where the inputs are the particle's impact velocity, η value, and embedded average particle size. In contrast, the predicted output metric is the percentage area coverage of the particles on the target surface. The embedded average particle size is measured 21 times for each spray condition, providing average and standard deviation values (Note: the Cu at 200 m/s particle size diameter was only measured 10 times since fewer particles were attached to the substrate). For the surface area coverage of particles, the SEM images of the as-CS samples were utilized and loaded into ImageJ software, which uses the threshold function for generating a black/white (particle) background. The threshold function was adjusted to produce the coated coverage areas. All measured values can be found in the Supporting Information of this study. As seen in Table 4, the embedded particles occupy the polymer surface area from <1 % to 100 %.

Notably, at the impact velocity of 200 m/s, the polymer substrate coverage area is <2 %. This statement is correct for both soft (Sn) and hard (Cu) particles, corresponding to the η value of <0.7. As the particle impact velocity is increased to 400 m/s, both particles remarkably cover the polymer substrate, resulting in an effective polymer metallization (see Fig. 5 a-c). At the impact velocity of 300 m/s, it is measured that the Sn average embedded particle size is 10.78 um with a standard deviation of 4.39 um, while the Cu average is 16.11 um with a standard deviation of 5.5 um, having the corresponding η values of 0.8 (for Sn) and 0.85 (for Cu). Taken together, the results reveal that the η value should be higher than 0.8 for an effective polymer metallization with insignificant porosity on the surface. As such, the η value can effectively serve as predictive metric for CS metallization on polymer targets. Furthermore, the findings confirm that the η value obtained from single-particle impingement studies can be effectively extrapolated to actual surface deposition, enabling high-fidelity prediction of CS polymer metallization.

Lastly, we compared our findings with the published literature in the domain of CS polymer metallization. Specifically, by incorporating the CS settings from these studies into the developed maps diagrams in Fig. 5, we calculated the relevant deposition probability (η) as seen in Table 5. The surface area coverage of particle (%) shows a strong correlation with the (η) value. Using the spray parameters from the cited paper, our (η) value has indicated the possibility of particles deposited on the polymer substrate relative to process parameters.

Future works may be directed toward incorporating (i) the CS gas temperature into the model; (ii) the effect of nozzle traverse speed on the deposition; (iii) multiple particles impact; (iv) evaluating η value as a metric to estimate and prevent substrate damage under high-speed particle impingement. The prospect of developing a predicting model would assist to control the spray process parameters for improved deposition efficiency.

5. Conclusion

This study developed a predictive modeling approach for CS metallization on polymer substrates by considering both soft (Sn) and hard (Cu) feedstock particles. Initially, the high-speed impingement of a single particle on a polymer target (Nylon) was modeled to simulate the CS metallization process. In the model, the high-strain plastic deformation of the polymer under the high-speed impinging metal particles was captured using the three-network (TNM) modeling, which is explicitly calibrated for the Nylon target. Following the modeling efforts, a non-dimensional number (η) was derived to establish a relationship between the kinetic energy fraction of the particle before and after impingement. Subsequently, the η value—representing the fraction of kinetic energy—was employed to predict the deposition probability, aligning with the microstructural characterization of the resulting CS metallization. Notably, effective CS metallization on polymers was predicted when η >0.8. This statement holds true for both soft and hard particles such as Sn and Cu. The model was then extrapolated to define a generalized CS metallization window on polymeric substrates by considering a comprehensive set of particles' physical properties, including density and diameter. In this context, the η value was correlated with the percentage area coverage of the as-CS particles on the polymer surface, enabling the development of a predictive tool for CS metallization. The results revealed that the η value should be higher than 0.8 to cover the polymer substrate with insignificant porosity. The developed modeling framework facilitates and streamlines CS parameters selection for an optimized process, minimizing the need for cost-intensive trial-and-error efforts.

Funding

This research is supported by NSTC 112-2222-E-011-003.

CRediT authorship contribution statement

Jung-Ting Tsai: Writing – original draft, Methodology, Investigation, Data curation, Conceptualization. **Semih Akin:** Writing – review & editing, Validation, Supervision. **David F. Bahr:** Supervision, Methodology. **Martin Byung-Guk Jun:** Supervision, Methodology.

Declaration of competing interest

The authors declare the following financial interests/personal relationships which may be considered as potential competing interests: Jung-Ting Tsai reports financial support was provided by National Science and Technology Council. If there are other authors, they declare that they have no known competing financial interests or personal relationships that could have appeared to influence the work reported in this paper.

Appendix A. Supplementary data

Supplementary data to this article can be found online at https://doi.org/10.1016/j.surfcoat.2024.130711.

References

[1] S. Yin, P. Cavaliere, B. Aldwell, R. Jenkins, H. Liao, W. Li, et al., Cold spray additive manufacturing and repair: fundamentals and applications, Addit. Manuf. 21 (2018) 628–650.
[2] F.S. da Silva, N. Cinca, S. Dosta, I.G. Cano, J.M. Guilemany, C.S.A. Caires, et al., Corrosion resistance and antibacterial properties of copper coating deposited by cold gas spray, Surf. Coat. Technol. 361 (2019) 292–301.
[3] Z. Khalkhali, J.P. Rothstein, Characterization of the cold spray deposition of a wide variety of polymeric powders, Surf. Coat. Technol. 383 (2020) 125251.
[4] Z. Khalkhali, W. Xie, V.K. Champagne, J.-H. Lee, J.P. Rothstein, A comparison of cold spray technique to single particle micro-ballistic impacts for the deposition of polymer particles on polymer substrates, Surf. Coat. Technol. 351 (2018) 99–107.
[5] P.C. King, A.J. Poole, S. Horne, R. de Nys, S. Gulizia, M.Z. Jahedi, Embedment of copper particles into polymers by cold spray, Surf. Coat. Technol. 216 (2013) 60–67.
[6] X.L. Zhou, A.F. Chen, J.C. Liu, X.K. Wu, J.S. Zhang, Preparation of metallic coatings on polymer matrix composites by cold spray, Surf. Coat. Technol. 206 (2011) 132–136.
[7] S. Akin, S. Lee, S. Jo, D.G. Ruzgar, K. Subramaniam, J.-T. Tsai, et al., Cold spray-based rapid and scalable production of printed flexible electronics, Addit. Manuf. 60 (2022) 103244.
[8] J.-T. Tsai, L.-K. Lin, S.-T. Lin, L. Stanciu, M.B.-G. Jun, The influence of Bi2O3 glass powder in the silver paste and the impact on silicon solar cell substrates, Mater. Des. 200 (2021) 109453.
[9] L.-K. Lin, J.-T. Tsai, S. Díaz-Amaya, M.R. Oduncu, Y. Zhang, P.-Y. Huang, et al., Antidelaminating, thermally stable, and cost-effective flexible Kapton platforms for nitrate sensors, mercury aptasensors, protein sensors, and p-type organic thin-film transistors, ACS Appl. Mater. Interfaces 13 (2021) 11369–11384.
[10] R. Lupoi, W. O'Neill, Deposition of metallic coatings on polymer surfaces using cold spray, Surf. Coat. Technol. 205 (2010) 2167–2173.
[11] A. Małachowska, M. Winnicki, Ł. Konat, T. Piwowarczyk, L. Pawłowski, A. Ambroziak, et al., Possibility of spraying of copper coatings on polyamide 6 with low pressure cold spray method, Surf. Coat. Technol. 318 (2017) 82–89.
[12] H. Wu, X. Xie, M. Liu, C. Chen, H. Liao, Y. Zhang, et al., A new approach to simulate coating thickness in cold spray, Surf. Coat. Technol. 382 (2019) 125151.
[13] A. Moridi, S.M. Hassani-Gangaraj, M. Guagliano, M. Dao, Cold spray coating: review of material systems and future perspectives, Surf. Eng. 30 (2014) 369–395.
[14] S. Akin, J.-T. Tsai, M.S. Park, Y.H. Jeong, M.B.-G. Jun, Fabrication of electrically conductive patterns on acrylonitrile-butadiene-styrene polymer using low-pressure cold spray and electroless plating, J. Micro Nano-Manuf. 8 (2021).
[15] J.-T. Tsai, D.F. Bahr, S. Akin, F. Zhou, M.B.-G. Jun, M. Park, Simulation and characterization of cold spray deposition of metal powders on polymer substrate electrically conductive application, in: ASME 2020 15th International Manufacturing Science and Engineering Conference, 2020.
[16] Y. Xie, C. Chen, M.-P. Planche, S. Deng, R. Huang, Z. Ren, et al., Strengthened peening effect on metallurgical bonding formation in cold spray additive manufacturing, J. Therm. Spray Technol. 28 (2019) 769–779.
[17] V. Gillet, E. Aubignat, S. Costil, B. Courant, C. Langlade, P. Casari, et al., Development of low pressure cold sprayed copper coatings on carbon fiber reinforced polymer (CFRP), Surf. Coat. Technol. 364 (2019) 306–316.
[18] S. Rahmati, A. Ghaei, The use of particle/substrate material models in simulation of cold-gas dynamic-spray process, J. Therm. Spray Technol. 23 (2013).
[19] X. Wang, J. Shi, Validation of Johnson-Cook plasticity and damage model using impact experiment, Int. J. Impact Eng. 60 (2013) 67–75.
[20] M. Murugesan, D.W. Jung, Johnson cook material and failure model parameters estimation of AISI-1045 medium carbon steel for metal forming applications, Materials 12 (2019) 609.
[21] F. Qin, T. An, N. Chen, Strain rate effect and Johnson-Cook models of lead-free solder alloys, in: 2008 International Conference on Electronic Packaging Technology & High Density Packaging, 2008, pp. 1–7.
[22] H. Cho, S. Bartyczak, W. Mock, M.C. Boyce, Dissipation and resilience of elastomeric segmented copolymers under extreme strain rates, Polymer 54 (2013) 5952–5964.
[23] H. Assadi, H. Kreye, F. Gärtner, T. Klassen, Cold spraying – a materials perspective, Acta Mater. 116 (2016) 382–407.
[24] R. Ghelichi, S. Bagherifard, M. Guagliano, M. Verani, Numerical simulation of cold spray coating, Surf. Coat. Technol. 205 (2011) 5294–5301.
[25] C.R. Siviour, S.M. W., J.E. F., P.H. P., N.A. S., High strain rate characterization of polymers, in: AIP Conference Proceedings vol. 1793, 2017 060029.
[26] H. Pouriayevali, Describing Large Deformation of Polymers at Quasi-static and High Strain Rates, 2013.
[27] C.R. Siviour, S.M. Walley, W.G. Proud, J.E. Field, The high strain rate compressive behaviour of polycarbonate and polyvinylidene difluoride, Polymer 46 (2005) 12546–12555.
[28] S. Sarva, A.D. Mulliken, M.C. Boyce, Mechanics of Taylor impact testing of polycarbonate, Int. J. Solids Struct. 44 (2007) 2381–2400.
[29] M.I. Okereke, C.P. Buckley, C.R. Siviour, Compression of polypropylene across a wide range of strain rates, in: Mechanics of Time-Dependent Materials vol. 16, 2012, pp. 361–379.
[30] C.R. Siviour, J.L. Jordan, High strain rate mechanics of polymers: a review, J. Dyn. Behav. Mater. 2 (March 01 2016) 15–32.
[31] P. Church, R. Cornish, I. Cullis, P. Gould, I. Lewtas, Using the split Hopkinson pressure bar to validate material models, Philos. Trans. R. Soc. A Math. Phys. Eng. Sci. 372 (2014) 20130294.
[32] J.-T. Tsai, M.B.-G. Jun, D.F. Bahr, Measurement methods for quantifying powder flowability and velocity in cold spray systems, Adv. Powder Technol. 34 (2023) 103910.
[33] J.-T. Tsai, S. Akin, F. Zhou, D.F. Bahr, M.B.-G. Jun, Establishing a cold spray particle deposition window on polymer substrate, J. Therm. Spray Technol. 30 (2021) 1069–1080.
[34] ASTM International, D638-14 Standard Test Method for Tensile Properties of Plastics, 2014 (ed. West Conshohocken, PA).
[35] J.-T. Tsai, Improving the Mechanical Properties of Cold Spray Metalized Polymers, Purdue University Graduate School, 2021.
[36] J. Bergstrom, J. Bischoff, An advanced thermomechanical constitutive model for UHMWPE, Int. J. Struct. Changes Solids 2 (2010) 31–39.
[37] C. Cheng, R. Mahnken, A modified Zerilli–Armstrong model as the asymmetric visco-plastic part of a multi-mechanism model for cutting simulations, Arch. Appl. Mech. 91 (2021) 3869–3888.
[38] G.Z. Voyiadjis, Y. Song, A. Rusinek, Constitutive model for metals with dynamic strain aging, Mech. Mater. 129 (2019) 352–360.
[39] D.L. Preston, D.L. Tonks, D.C. Wallace, Model of plastic deformation for extreme loading conditions, J. Appl. Phys. 93 (2003) 211–220.
[40] H. Sedaghat, W. Xu, L. Zhang, C. Gao, W. Lu, W. Liu, 0610 A comparative study on Gao-Zhang and Johnson-Cook constitutive models, in: Proceedings of International Conference on Leading Edge Manufacturing in 21st century: LEM21 2015.8, 2015 (pp. _0610-1_-_0610-5_).
[41] Z. Guo, X. Shi, Y. Chen, H. Chen, X. Peng, P. Harrison, Mechanical modeling of incompressible particle-reinforced neo-Hookean composites based on numerical homogenization, Mech. Mater. 70 (2014) 1–17.
[42] E.M. Arruda, M.C. Boyce, Evolution of plastic anisotropy in amorphous polymers during finite straining, Int. J. Plast. 9 (1993) 697–720.
[43] E.M. Arruda, M.C. Boyce, A three-dimensional constitutive model for the large stretch behavior of rubber elastic materials, J. Mech. Phys. Solids 41 (1993) 389–412.
[44] J.S. Bergström, S.M. Kurtz, C.M. Rimnac, A.A. Edidin, Constitutive modeling of ultra-high molecular weight polyethylene under large-deformation and cyclic loading conditions, Biomaterials 23 (2002) 2329–2343.
[45] A. Almomani, S. Deveci, A.-H.I. Mourad, I. Barsoum, Constitutive model calibration for the thermal viscoelastic-viscoplastic behavior of high density polyethylene under monotonic and cyclic loading, Polym. Test. 118 (2023) 107911.
[46] J.-T. Tsai, S. Akin, F. Zhou, M.S. Park, D.F. Bahr, M.B.-G. Jun, Electrically conductive metallized polymers by cold spray and co-electroless deposition, ASME Open J. Eng. 1 (2022).
[47] T. Gabor, S. Akin, M.B.-G. Jun, Numerical studies on cold spray gas dynamics and powder flow in circular and rectangular nozzles, J. Manuf. Process. 114 (2024) 232–246.